Supporting Information

Imaging plasma membrane phase behaviour in live cells using a thiophene-based molecular rotor

Michael R. Dent,[a] Ismael López-Duarte,[a, b] Callum J. Dickson,[c] Phoom Chairatana,[b] Harry L. Anderson,[b] Ian R. Gould,[a] Douglas Wylie,[a] Aurimas Vyšniauskas,[a] Nicholas J. Brooks[a]* and Marina K. Kuimova[a]*

[a] Department of Chemistry, Imperial College London, Exhibition Road, London, SW7 2AZ, UK.

[b] Department of Chemistry, Oxford University, Chemistry Research Laboratory, Oxford, UK OX1 3TA

[c] Computer-Aided Drug Discovery, Global Discovery Chemistry, Novartis Institutes for BioMedical Research, 100 Technology Square, Cambridge, MA 02139, USA.

Correspondence to: m.kuimova@imperial.ac.uk; n.brooks@imperial.ac.uk; callum.dickson@novartis.com

Table of Contents for Supporting Information

(1) Materials and Methods

All solvents were purchased from Sigma-Aldrich or VWR and used without further purification. All lipids were obtained from Avanti Polar Lipids. The thiophene-based dye, **1**,[1] and the BODIPY-based molecular rotor, BODIPY++,[2] were synthesised as described elsewhere.

Emission spectra were taken using a Horiba Jobin Yvon Fluoromax 4. Lifetime measurements were obtained using a Horiba Jobin Yvon IBH 5000 F time-correlated single photon counting (TCSPC) device, using a pulsed NanoLED source at 467 nm. All TCSPC measurements gave 10,000 counts in the peak channel, and DAS software was used for fitting the decays. Decays were fitted with a biexponential function ($\chi^2 < 1.5$ in all cases). Unless otherwise stated, all spectra were taken at 298 K.

All bilayer studies used a maximum **1** concentration of 0.5 mol% (1:200 rotor:lipid) to prevent dye aggregation and to avoid significant disruption of the bilayer structure. Large unilamellar vesicles (LUVs) were formed using the gas extrusion method.[3] A solution of the appropriate lipid and **1** was prepared in chloroform, which was then evaporated off under nitrogen. Multilamellar vesicles (MLVs) were then prepared by hydrating the lipid film using enough water to give a 1 mM solution of lipid and vortexing for 1 minute above the gel transition temperature of the lipid. This was then extruded 10 times through a polycarbonate membrane with a pore diameter of 200 nm using a LIPEX extruder (Northern Lipids Inc., Canada), ensuring it was above the gel transition temperature of the lipid.

Giant unilamellar vesicles (GUVs) were prepared using the electroformation method.[4] A solution of 1 $mg.mL^{-1}$ lipid with dye **1** in chloroform was added dropwise (ca. 30 µL) onto a clean conductive indium tin oxide (ITO) coated glass slide and spread using a glass coverslip to give a thin film of lipid and **1**, before being lyophilised for 60 minutes. A polydimethyl siloxane (PDMS) spacer was placed over the lipid film and a second ITO coated slide was then placed on top of the spacer, creating a sealed chamber. The chamber was filled with 0.1 M aqueous sucrose solution using a syringe. An AC voltage of 1.0 V and 10 Hz was applied for 90 minutes, making sure the chamber was held above the gel transition temperature of the lipids being used. In order to be visible in phase contrast microscopy, the GUVs formed in this way were suspended in a 0.125 M aqueous solution of glucose.

FLIM measurements were performed on a Leica TSC SP5 II inverted confocal microscope with a 63x water immersion objective (NA = 1.2). A multiphoton laser was used for excitation, using two-photon excitation at 900 nm. Decay traces were analysed using SPCimage software, which was used to fit decay traces in order to give lifetime values. All images were binned to give a minimum of 300 counts per pixel before fitting.

Molecular dynamics simulations were performed using the AMBER suite.[5] See section (3) of the supporting information for further details of the molecular dynamics simulations.

Live cells (BE, HCT 116, NIH 3T3 or neuroblastoma lines) suspended in a solution of trypsin (1 mL) were quenched with media (5 mL; DMEM, Sigma, 10% FBS, 1% PS, 1 LG) and 10 µL of the solution was placed into a haemocytometer and counted under magnification.

Enough of this solution was added to each well of Lab-Tek Chamber slides (borosilicate glass) to give 4 x 10^4 cells per well. The wells were incubated overnight in DMEM medium prior to microscopy studies. For imaging, the cells were incubated in DMEM containing 1-10 μM of **1** before washing with HBSS and imaging.

Phasor analysis was done using in-house software written in Matlab (MathWorks). Phasor analysis was performed by taking a Fourier transform of the fluorescence decay and plotting the real (g) versus the imaginary (s) component of the Fourier transform. The components are calculated using the following equations:

$$g(\omega) = \frac{\int_0^\infty I(t)\cos(\omega t)dt}{\int_0^\infty I(t)dt}$$

$$s(\omega) = \frac{\int_0^\infty I(t)\sin(\omega t)dt}{\int_0^\infty I(t)dt}$$

Where I(t) is the fluorescence decay, ω is the angular frequency (2*π*80 MHz) and *t* is time. If the fluorescence decay is monoexponential, the point produced by a phasor transform lies on the semicircle centred at g = 0.5, s = 0. In the case of multiexponential decay, the point lies within a semicircle. The phasor transform of a FLIM image produces a cloud of points where the points correspond to the individual decays in the FLIM image. In our work (Fig. 7), we show the centres of the clouds for clarity.

(2) Fluorescence properties of 1 in LUVs

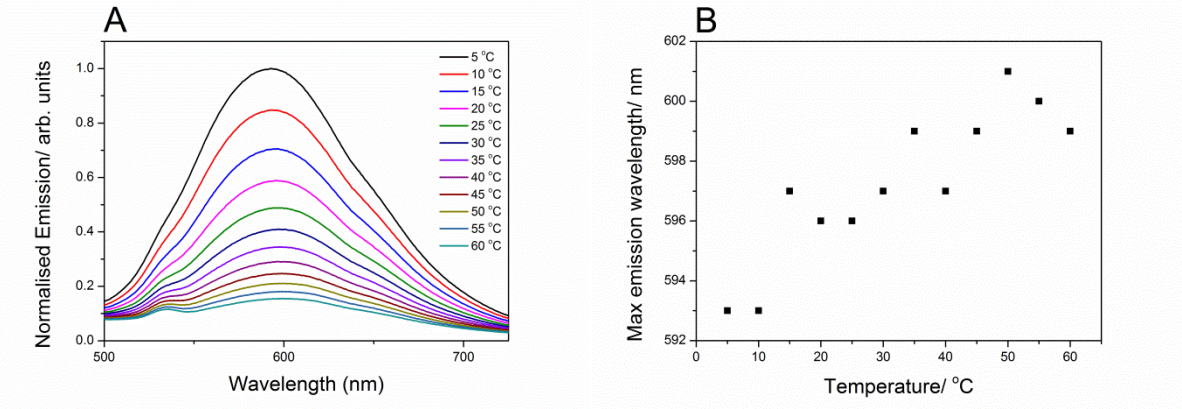

Fig. S1 – (A) Overlaid emission spectra of **1** in DOPC LUVs at a range of temperatures, (B) max emission wavelength of **1** in DOPC as a function of temperature

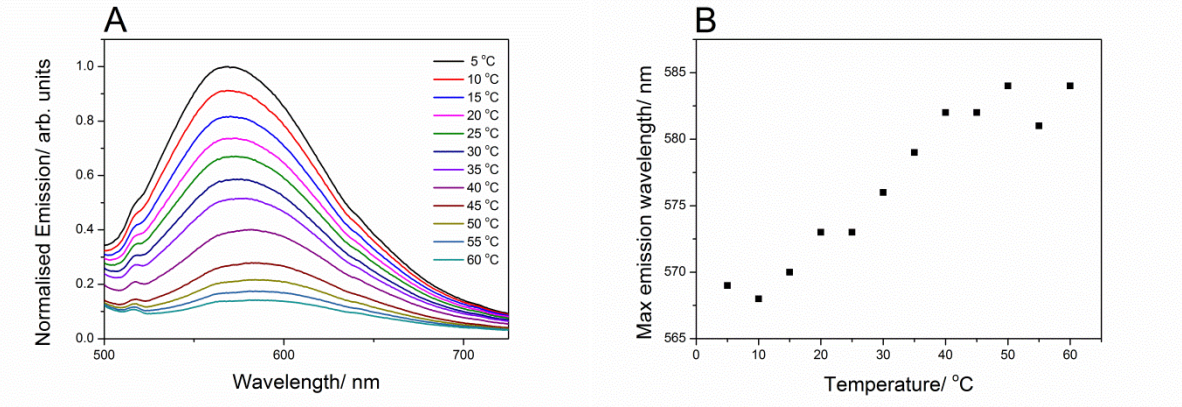

Fig. S2 – (A) Overlaid emission spectra of **1** in DPPC LUVs at a range of temperatures, (B) max emission wavelength of **1** in DPPC as a function of temperature

Dye **1** has previously[1] been shown to display solvatochromic emission, with maximum emission wavelength increasing with solvent polarity. In both DOPC and DPPC LUVs, emission wavelength increases at higher temperatures, which may reflect an increased water penetration into the bilayer at increased temperature.

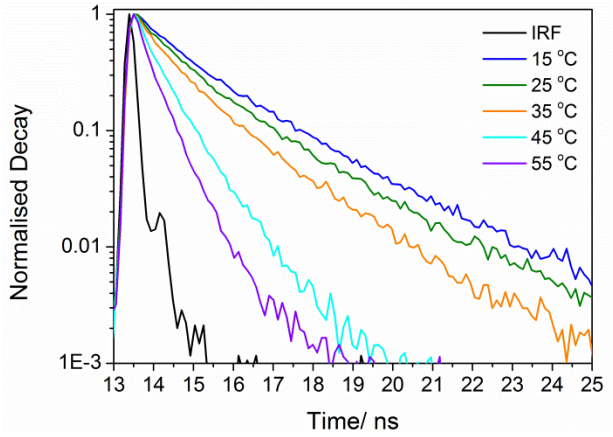

Fig. S3 – Normalised fluorescence decays of **1** in DPPC LUVs at a range of temperatures.

A large difference in lifetime can be observed between 35 and 40 ^{0}C. This reflects the viscosity change[6] associated with the phase transition between the gel and liquid phase of the DPPC bilayer.

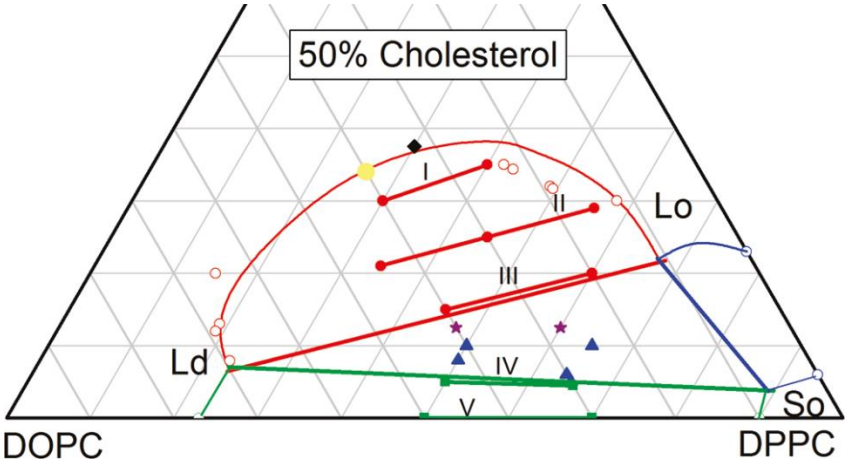

Fig. S4 – Phase diagram for DOPC, DPPC and cholesterol (reproduced from[7])

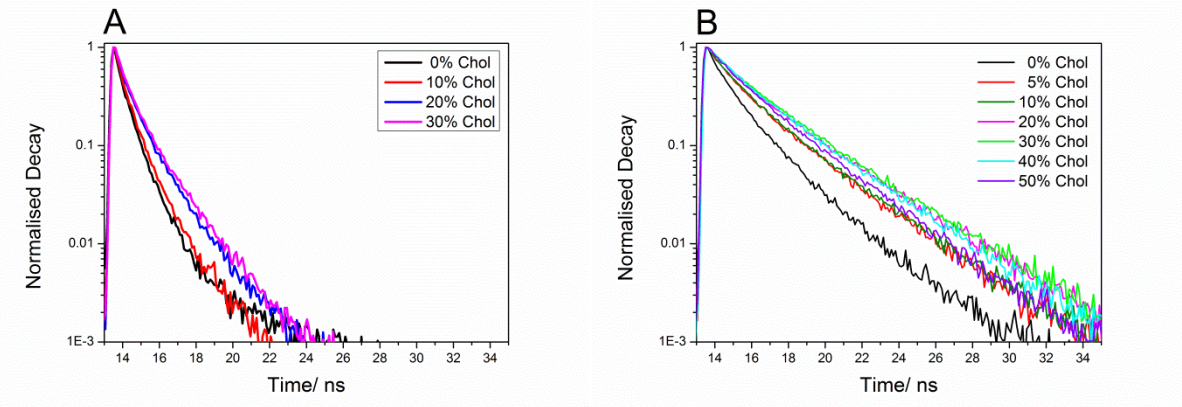

Fig. S5 – Decays of **1** in LUVs of (A) DOPC and (B) DPPC with varying concentrations of cholesterol

We have recorded time resolved fluorescence decays of **1** in LUVs composed of DOPC and DPPC with varying concentrations of cholesterol, shown in Fig. S5. In both cases, addition of cholesterol causes an increase in lifetime of **1**. Whilst cholesterol is known to increases lipid ordering of unsaturated lipids[8] such as DOPC, leading to an increase in viscosity[6], it decreases lipid ordering within gel phase bilayers[8], meaning that a decreased viscosity so a decreased lifetime of **1** would be expected. This is clearly not the case here, with lifetime of **1** increasing with increasing cholesterol content. We have performed molecular dynamic simulations, section **(3)**, and demonstrated that the addition of cholesterol causes a bilayer relocation of **1**, which explains the unexpected increase in lifetime observed above. The possibility to adopt multiple orientations in a DPPC bilayer upon the addition of cholesterol was further confirmed by the variable width of the fluorescence spectra of **1** recorded in lipid mixtures of DPPC with cholesterol, Fig. S6.

Table S1 – Mean-weighted lifetimes of **1** in DOPC and DPPC LUVs with cholesterol content

	DPPC	DOPC
% Cholesterol	Mean Weighted Lifetime/ ps	Mean Weighted Lifetime/ ps
0	2190	970
5	2900	
10	2930	990
20	3380	1300
30	3350	1410
40	3180	
50	2910	

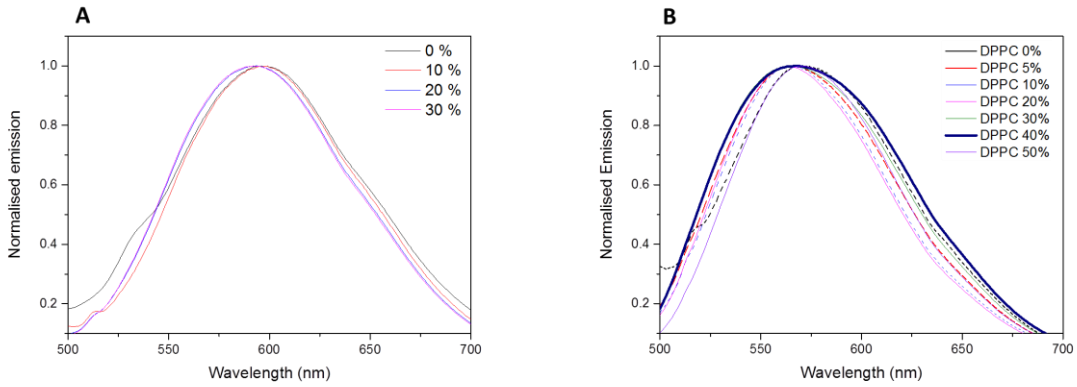

Fig. S6 – Emission spectra of **1** in DOPC (A) and DPPC (B) LUVs at different cholesterol concentrations. In (A), the dashed lines represent 0%, 5% and 10% cholesterol

(3) Molecular Dynamics Simulations

METHODS

The following systems were constructed consisting of 128 lipids total: DOPC membranes containing 0%, 10%, 20%, 30%, 40% and 50% molar fraction of cholesterol; and DPPC membranes containing 0%, 10%, 20%, 30%, 40% and 50% molar fraction of cholesterol. Each system was solvated by 40 waters per lipid and had four dye **1** molecules in the upper membrane layer. Eight chloride ions were added to the water layer to achieve charge neutrality of the systems. The dye **1** molecules were modelled using the General Amber Force Field,[9] lipids and cholesterol using the Lipid14 force field,[10–13] water by the TIP3P model,[14] and ions by Joung et al.[15]

All systems underwent an identical equilibration and simulation protocol using AMBER14 and PMEMD CUDA.[5,16,17] First, the system was energy minimized for 10000 steps, of which the first 5000 steps used the steepest descent method and the remaining steps used the conjugate gradient method.[18] The system was then heated from 0 K to 100 K using Langevin dynamics[19] within a 5 ps constant volume run, with restraints on the lipids and **1** (force constant 10 kcal/mol/Å^2). All restraints were then removed, the volume was then allowed to change freely and the temperature increased to 323 K (DPPC systems) or 303 K (DOPC systems) with a Langevin collision frequency of γ=1 ps^{-1}, and anisotropic Berendsen control of the pressure[20] around 1 atm was applied by coupling the periodic box with a time constant of 2 ps for 100 ps.

All systems were then run at constant pressure (NPT) for 100 ns to allow equilibration. Three dimensional periodic boundary conditions with the usual minimum image convention were employed. Bonds involving hydrogen were constrained using the SHAKE algorithm,[21] allowing a 2 fs time-step. Particle mesh Ewald was used to treat all electrostatic interactions[22] beyond a cut-off of 10 Å. A long-range analytical dispersion correction was applied to energy and pressure.

Following equilibration, each system was slowly cooled to 296 K over 15 ns and systems left to run for a further 100 ns at 296 K. Finally, production runs of 100 ns were performed at constant pressure and constant temperature of 296 K. Trajectory coordinates were recorded every 10 ps. Four repeats of each system were run; results are thus an average over four runs of 100 ns with standard deviation.

All analysis was performed with CPPTRAJ;[23] molecular modelling Fig.s were generated with VMD[24]. To quantify the orientation of the dye molecules inside the membrane during the course of the simulations, the molecular order parameter (P_2) of each molecule of **1** was monitored using the angle θ between the long axis of inertia of the molecule and the membrane normal (z-axis).

$$\boldsymbol{P_2 = \frac{1}{2}\langle 3cos^2\theta - 1\rangle} \quad \text{Equation S1}$$

P_2 can take a value between 1 (indicating orientation with the membrane normal i.e. aligned with lipid tails) and -0.5 (indicating alignment with membrane plane). A value of 0 indicates random orientation.

RESULTS

DOPC + 1 simulations

The electron density profiles from the production simulations of the DOPC membrane systems containing four dye **1** molecules and increasing molar fractions of cholesterol are shown in Fig. S7. These allow time-averaged spatial resolution of each molecular component in the system. The dye **1** signal has been scaled up to aid interpretation.

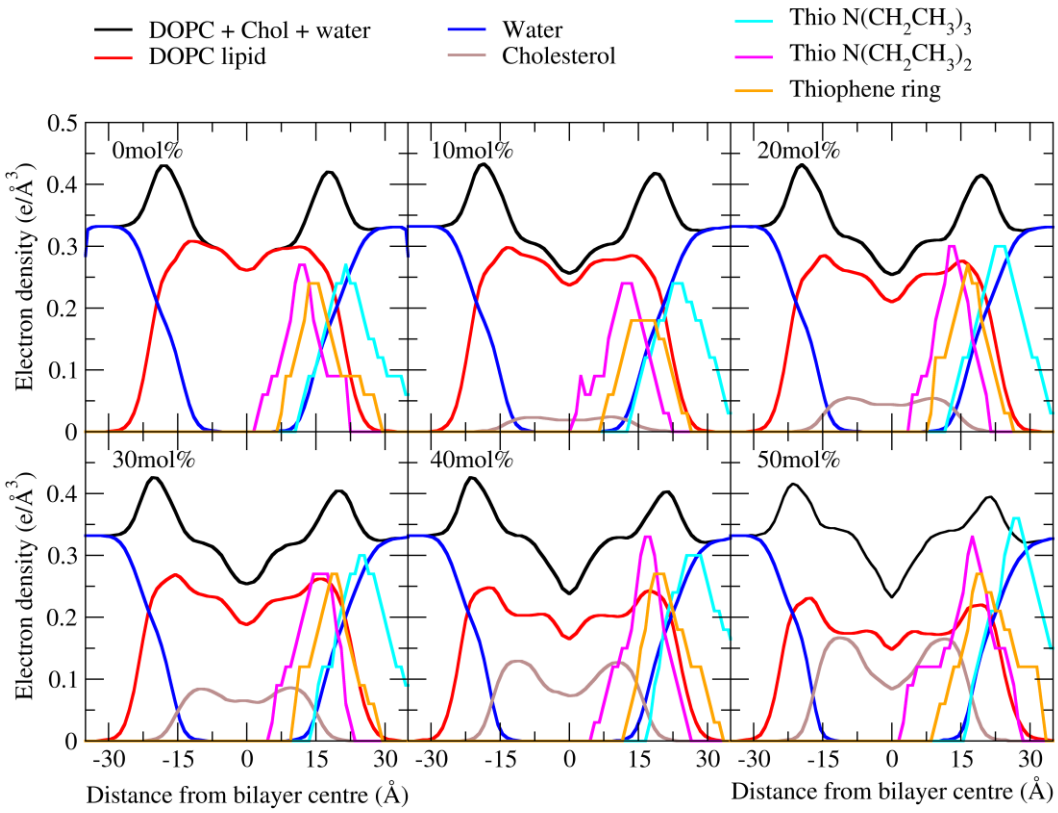

Fig. S7 – Electron density profiles from simulations of DOPC membranes containing four molecules of **1** and increasing molar fractions of cholesterol.

From the electron density profiles, the orientation of the dye molecules does not appear to change greatly in DOPC membranes with increasing content of cholesterol. However, they do appear to be pushed slightly upward and out of the membrane as cholesterol is added.

The average P_2 order parameter value of dye molecules in a DOPC membrane with increasing cholesterol content is shown in Fig. S8. The order parameter values have been grouped as greater than P_2=0.25 i.e. the angle between dye **1** and membrane normal is above 45°; or below P_2=0.25 i.e. the angle between dye **1** and membrane normal is below 45°. Each symbol is scaled by the number of dye **1** molecules within the group.

It can be seen from Fig. S8 that there is a roughly equal split (at least, for 30 mol% cholesterol and above) between molecules of **1** slightly aligned with the membrane normal and a random alignment. For 0-20 mol% cholesterol there does not appear to be a trend – the dye molecules sample different orientations.

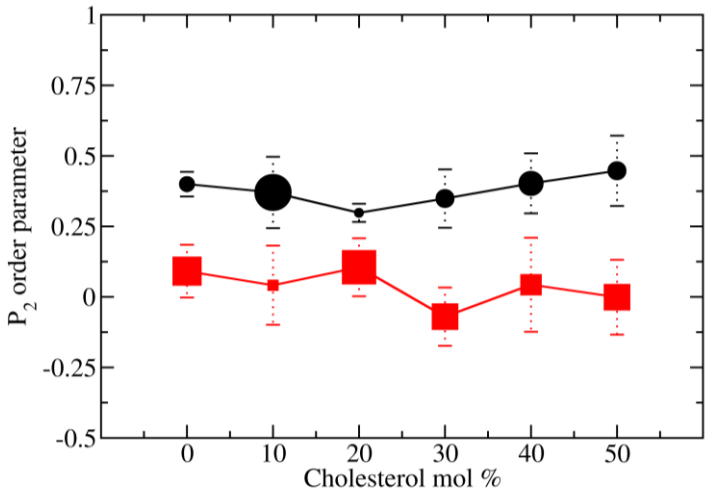

Fig. S8 – Average dye **1** order parameter from DOPC membrane simulations containing increasing molar fraction of cholesterol. P_2 values have been grouped into >0.25 (black) or <0.25 (red). Furthermore, the size of each symbol has been scaled by the number of dye **1** molecules in each group.

DPPC + 1 simulations

The electron density profiles from the production simulations of the DPPC membrane systems containing four dye **1** molecules and increasing fractions of cholesterol are shown in Fig. S9.

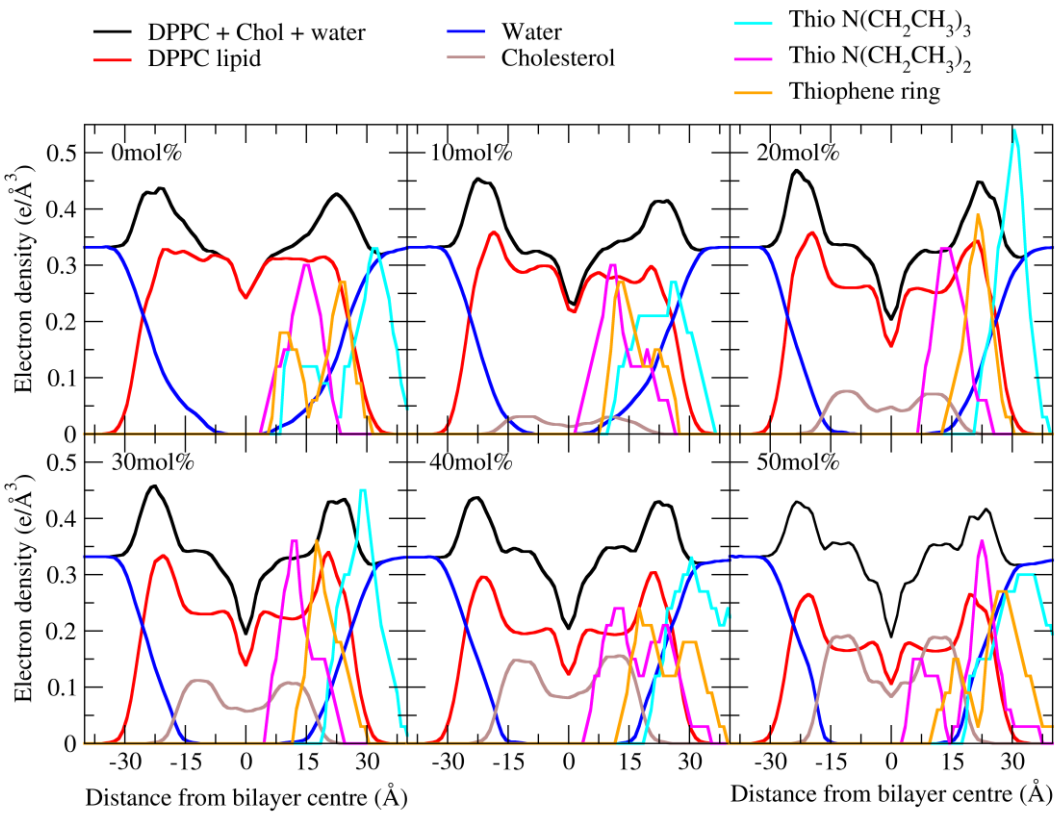

Fig. S9 – Electron density profiles from simulations of DPPC membranes containing four dye **1** molecules and increasing molar fractions of cholesterol.

From Fig. S9, it is observed that the dye **1** orientation does vary with increasing cholesterol content. Above 30 mol% molar fraction of cholesterol the dye transitions from orientation of aligned along the membrane normal to aligned along the membrane plane. Consequently, at 40 and 50 mol% there is a mixture of dye alignments – the signal remains for dye molecules aligned along the membrane normal, yet a new signal appears for dye aligned along the plane.

It can be concluded that there are two preferred orientations at high cholesterol content versus a single preferred orientation at zero/low cholesterol content.

The average P_2 order parameter value of dye molecules in a DPPC membrane with increasing molar fraction of cholesterol reinforces conclusions from the electron density profiles (see Fig. S10). At 0 and 10 mol% cholesterol the majority of dye **1** molecules are aligned along the membrane normal, with a small number aligned along the membrane plane. At 20 mol%, all dye **1** molecules are aligned along the membrane normal (with low fluctuation, note the smaller error bars). Starting at 30 mol% the number of dye **1** molecules aligned with the membrane normal steadily decreases, at the same time the number of dye **1** molecules transitioning to alignment with the membrane plane concurrently increases. Overall, we see a shift from dye **1** molecules predominantly aligned along membrane normal to dye **1** molecules predominantly adopting random / aligned along membrane plane orientation starting at 30 mol% cholesterol.

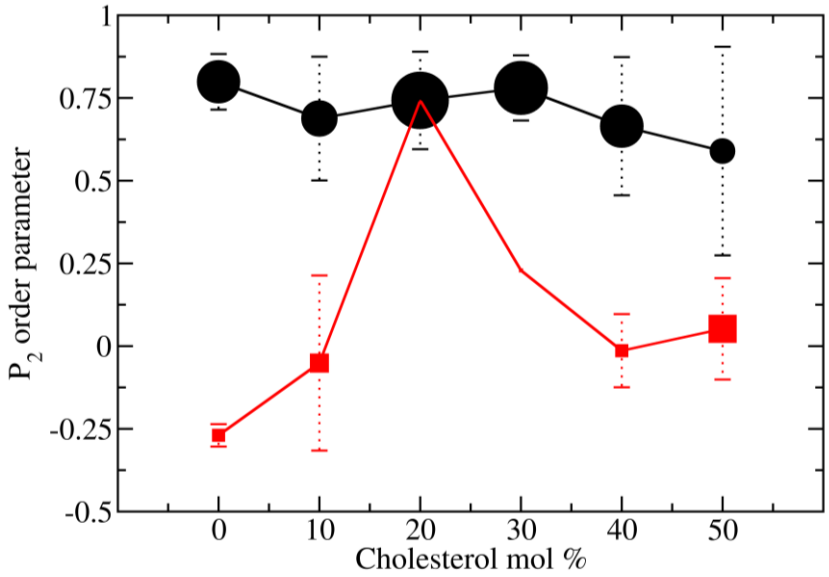

Fig. S10 – Average dye **1** order parameter from DPPC membrane simulations containing increasing molar fraction of cholesterol. P_2 values have been grouped into >0.25 (black) or <0.25 (red). Furthermore, the size of each symbol has been scaled by the number of dye molecules in each group.

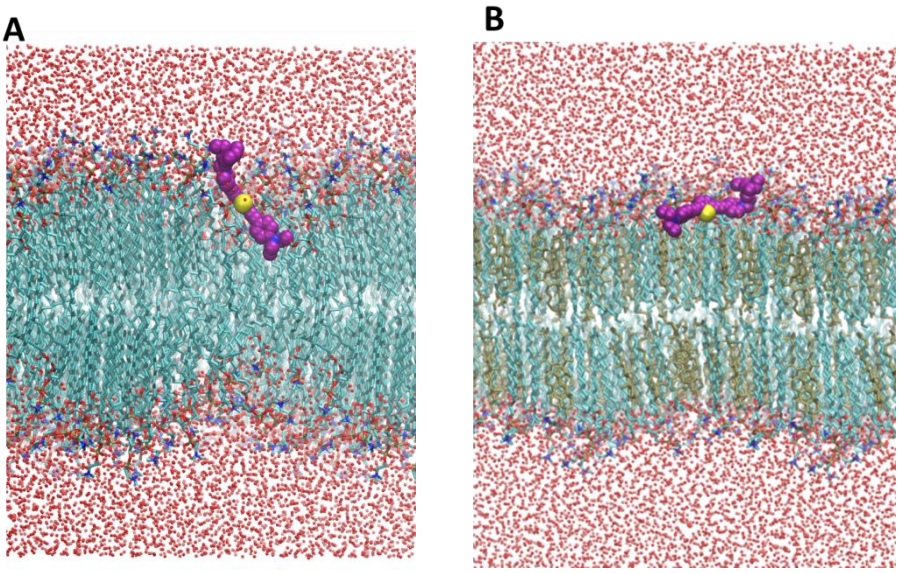

Fig. S11 – (A) dye **1** in DPPC at 0 mol% cholesterol, (B) dye **1** in DPPC at 50 mol% cholesterol

These simulations show a large scale bilayer rearrangement of **1** with increasing cholesterol for DPPC. This may explain the increase in fluorescence lifetime of **1** in DPPC with increasing cholesterol, despite the decreasing membrane ordering and viscosity.

Temperature effect

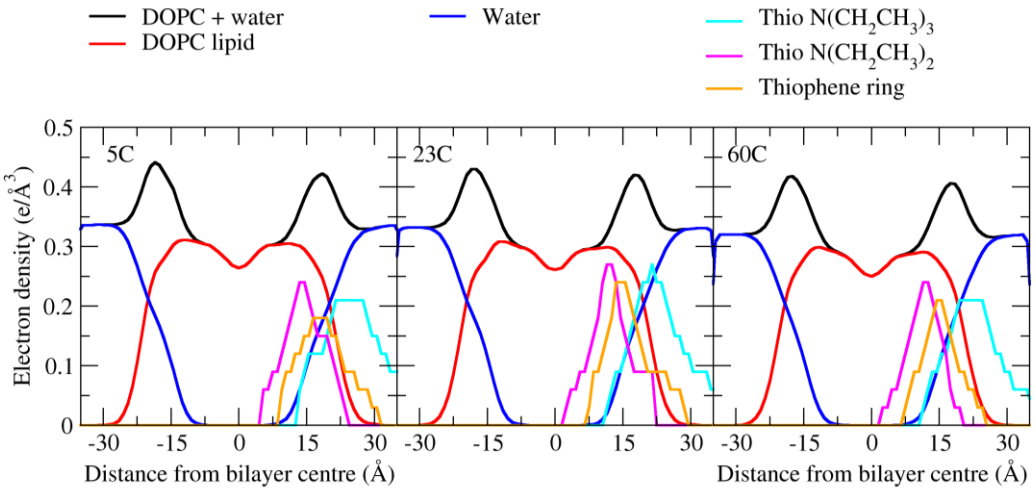

Fig. S12– The effect of temperature on the positioning of **1** in a DOPC bilayer with 0mol% cholesterol (four dye **1** molecules considered at 5 ºC, 23 ºC and 60 ºC)

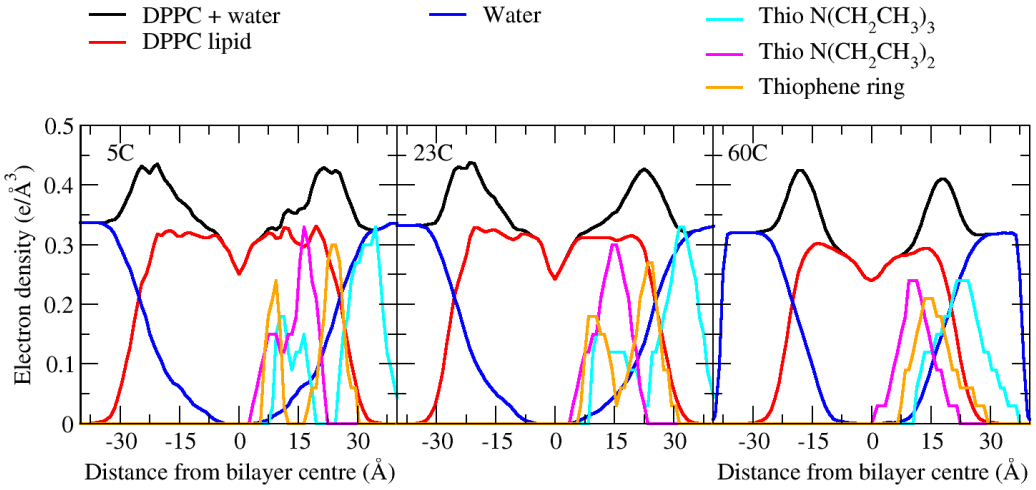

Fig. S13 - The effect of temperature on the positioning of **1** in a DPPC bilayer with 0mol% cholesterol (four dye **1** molecules considered at 5 ºC, 23 ºC and 60 ºC)

Fig. S12 and S13 demonstrate that there is no discernible effect of temperature on the positioning of **1** in DOPC and DPPC bilayers.

The positioning of 1 vs BODIPY++ in the bilayer

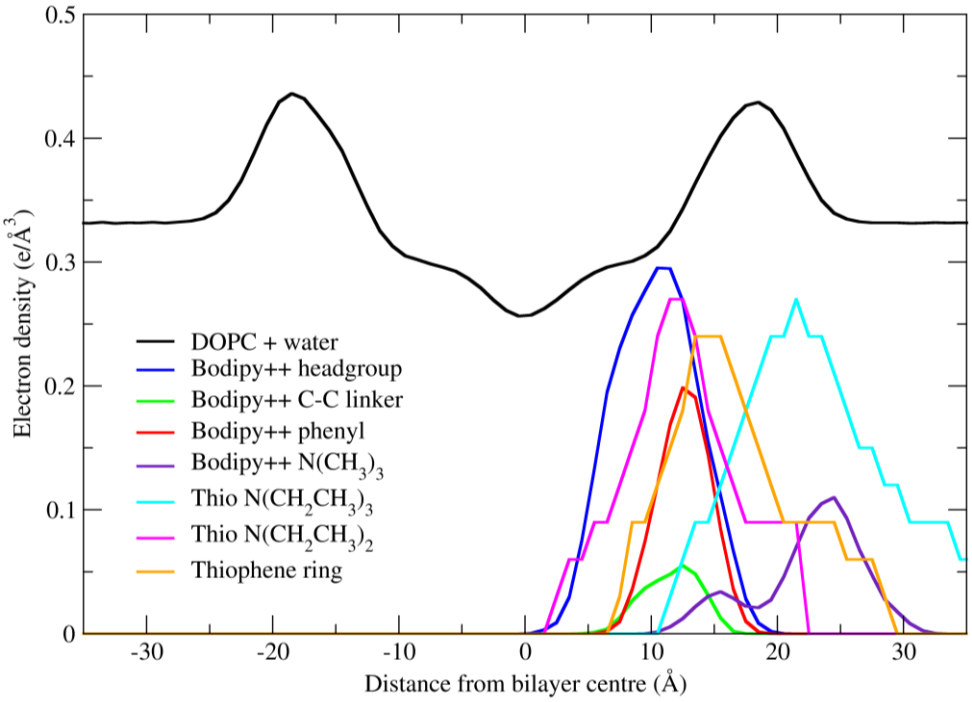

Fig. S14 - BODIPY++ (structure shown in Fig. S15)[6] in DOPC versus dye **1** in DOPC

By comparing the orientation of **1** in the DOPC bilayer with that of a well-studied BODIPY rotor,[6] we found that the rotating units of the two dyes occupy essentially the same position within bilayer (Fig. S14).

Therefore, using the viscosity derived from the lifetime of the BODIPY rotor for the calibration of responses of **1** to viscosity (Fig. 2 main text) is, indeed, valid.

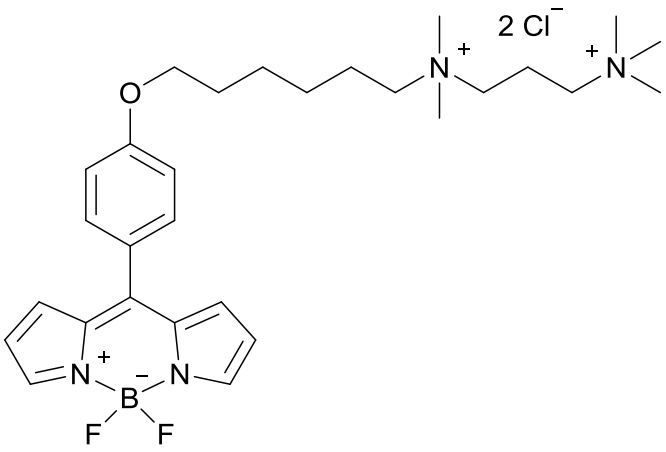

Fig. S15 Structure of BODIPY++

(4) 1 in phase-separated GUVS
DOPC/DPPC/cholesterol (1:1:1)

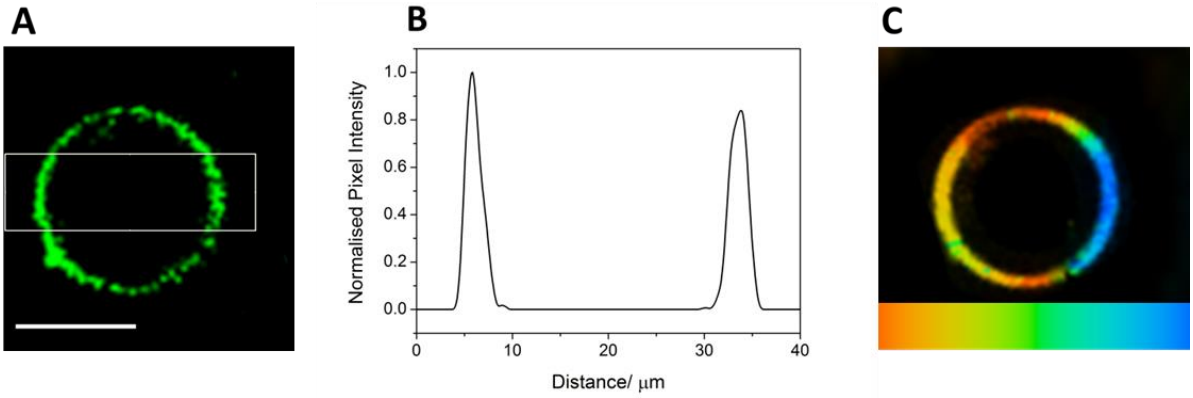

Fig. S16 – (A) Fluorescence confocal image of a phase separated GUV (DOPC/DPPC/cholesterol 1:1:1) with a cross section along the white rectangle shown in (B) giving approximately equal fluorescence intensity in both bilayer locations. The FLIM image of the same GUV is shown in (C) showing that the rectangle intersects the GUV in L_d (left, lower viscosity) and L_o (right, higher viscosity) phases, respectively. This data demonstrates equal partitioning of the rotor between the two phases.

DOPC/EYSM/Chol (1:1:1)

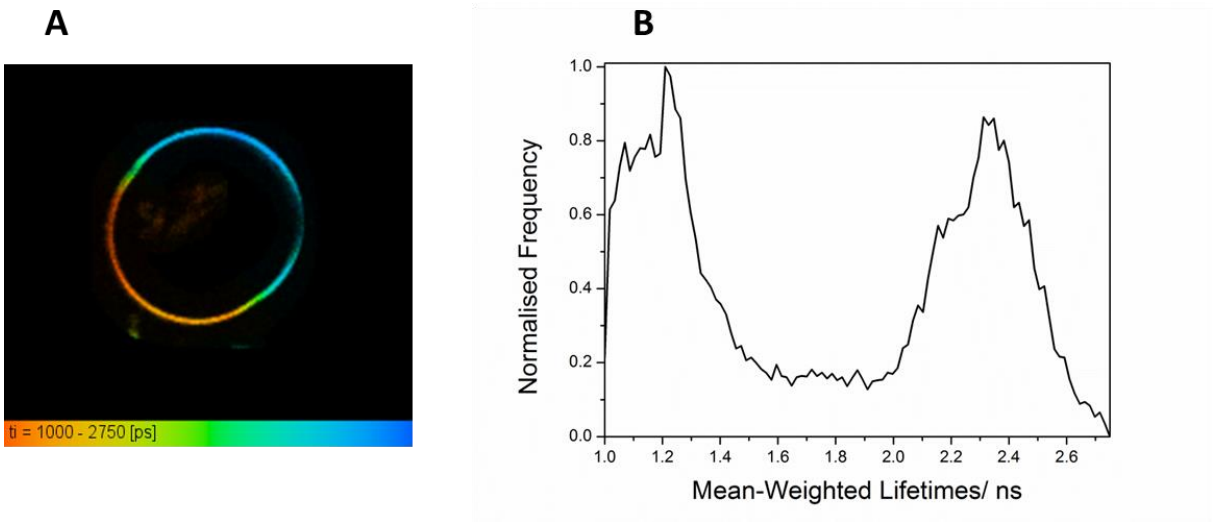

Fig. S17 – Sample lifetime image of **1** in a 1:1:1 DOPC/EYSM (egg sphingomyelin)/Cholesterol GUV and a lifetime distribution histogram of **1** in 10 GUVs consisting of 1:1:1 DOPC/EYSM/Cholesterol.

A similar effect on **1** is observed for this GUV composition as compared with the DOPC/DPPC/Cholesterol GUVs shown in main text, Fig. 5 and in Fig. S16. Again, **1** partitions equally between L_o and L_d phases, with a noticeable lifetime difference between the phases. In this case, the lifetime of the L_o phase is higher than in the DOPC/DPPC/Cholesterol GUVs.

(5) 1 in live cells

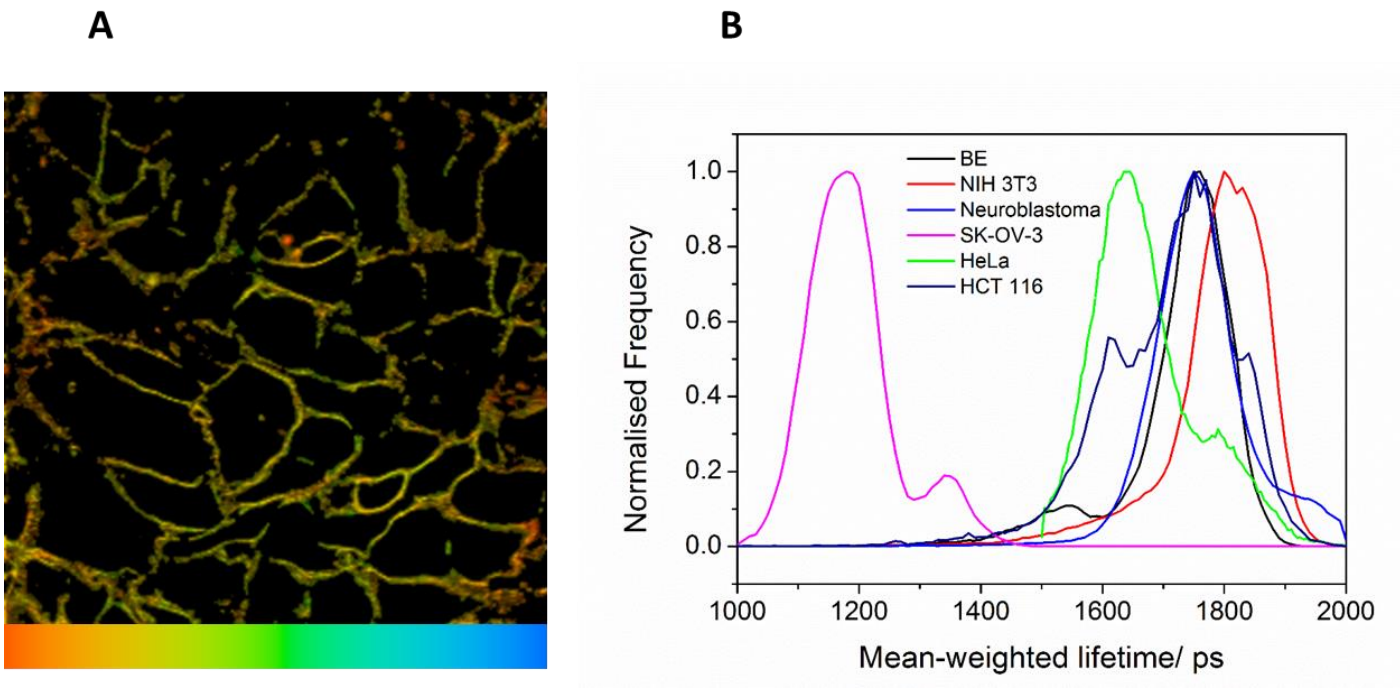

Fig. S18. (A) Sample fluorescence lifetime image of SK-OV-3 incubated with **1**; the colour hue mean-weighted lifetime range is between 1250-2150 ps; (B) histograms of a mean weighted lifetime showing distribution for the six cell lines used (BE, HCT 116, NIH 3T3, neuroblastoma, HeLa and SK-OV-3), averaged over 10 images.

The mean lifetimes for BE, HCT 116, NIH 3T3, neuroblastoma, HeLa and SK-OV-3 cell membranes are and 1725, 1710, 1786 1758, 1671 and 1378 ps, respectively. This data demonstrates that various live cell membranes show a range of rotor lifetimes (a range of viscosities), probably dependent on their cholesterol content. Even though the data from SK-OV-3 cells is a low-lying outlier (Fig. S18), these mean lifetime values of **1** in all cells are between values expected for L_o and L_d phases from studies in model membranes, and imply a mixture of coexisting L_o and L_d phases within each pixel of the lifetime image, albeit to a different extent in different cell lines.

(6) References

1. I. López-Duarte, P. Chairatana, Y. Wu, J. Pérez-Moreno, P. M. Bennett, J. E. Reeve, I. Boczarow, W. Kaluza, N. A. Hosny, S. D. Stranks, R. J. Nicholas, K. Clays, M. K. Kuimova, and H. L. Anderson, *Org. Biomol. Chem.*, 2015, **13**, 3792–3802.

2. I. López-Duarte, T. T. Vu, M. A. Izquierdo, J. A. Bull, and M. K. Kuimova, *Chem. Commun.*, 2014, **50**, 5282–5284.

3. L. D. Mayer, M. J. Hope, and P. R. Cullis, *Biochim. Biophys. Acta*, 1986, **858**, 161–168.

4. L. A. Bagatolli, T. Parasassi, and E. Gratton, *Chem. Phys. Lipids*, 2000, **105**, 135–147.

5. D. A. Case, V. Babin, J. T. Berryman, R. M. Betz, Q. Cai, D. S. Cerutti, T. E. Cheatham III, T. A. Darden, R. E. Duke, H. Gohlke, A. W. Goetz, S. Gusarov, N. Homeyer, P. Janowski, J. Kaus, I. Kolossváry, A. Kovalenko, T. S. Lee, S. LeGrand, T. Luchko, R. Luo, B. Madej, K. M. Merz, F. Paesani, D. R. Roe, A. Roitberg, C. Sagui, R. Salomen-Ferrer, G. Seabra, G. L. Simmerling, W. Smith, J. Swails, R. C. Walker, J. Wang, R. M. Wolf, X. Wu, and P. A. Kollman, *AMBER 14*, 2014, University of California, San Francisco.

6. M. R. Dent, I. López Duarte, C. J. Dickson, N. D. Geoghegan, J. M. Cooper, I. R. Gould, R. Krams, J. A. Bull, N. J. Brooks, and M. K. Kuimova, *Phys. Chem. Chem. Phys.*, 2015, **17**, 18393–18402.

7. P. Uppamoochikkal, S. Tristram-Nagle, and J. F. Nagle, *Langmuir*, 2010, **26**, 17363–17368.

8. H. Ohvo-Rekilä, B. Ramstedt, P. Leppimäki, and J. P. Slotte, *Prog. Lipid Res.*, 2002, **41**, 66–97.

9. J. M. Wang, R. M. Wolf, J. W. Caldwell, P. A. Kollman, and D. A. Case, *J. Comput. Chem.*, 2004, **25**, 1157–1174.

10. Å. A. Skjevik, B. D. Madej, R. C. Walker, and K. Teigen, *J. Phys. Chem. B*, 2012, **116**, 11124–11136.

11. C. J. Dickson, L. Rosso, R. M. Betz, R. C. Walker, and I. R. Gould, *Soft Matter*, 2012, **8**, 9617–9627.

12. C. J. Dickson, B. D. Madej, Å. A. Skjevik, R. M. Betz, K. Teigen, I. R. Gould, and R. C. Walker, *J. Chem. Theory Comput.*, 2014, **10**, 865–879.

13. B. D. Madej, I. R. Gould, and R. C. Walker, *J. Phys. Chem. B*, 2015, **119**, 12424–12435.

14. W. L. Jorgensen, J. Chandrasekhar, J. D. Madura, R. W. Impey, and M. L. Klein, *J. Chem. Phys.*, 1983, **79**, 926–935.

15. I. S. Joung and T. E. Cheatham III, *J. Phys. Chem. B*, 2008, **112**, 9020–9041.

16. A. W. Götz, M. J. Williamson, D. Xu, D. Poole, S. Le Grand, and R. C. Walker, *J. Chem. Theory Comput.*, 2012, **8**, 1542–1555.

17. R. C. Salomon-Ferrer, R., Götz, A. W., Poole, D., Le Grand, S., Walker, *J. Chem. Theory Comput.*, 2013, **9**, 3878–3888.

18. W. H. Press, S. A. Teukolsky, W. T. Vetterling, and B. P. Flannery, *Numerical Recipes: The Art of Scientific Computing*, Cambridge University Press, New York, Third Edit., 2007.

19. R. W. Pastor, B. R. Brooks, and A. Szabo, *Mol. Phys.*, 1988, **65**, 1409–1419.

20. H. J. C. Berendsen, J. P. M. Postma, W. F. van Gunsteren, A. DiNola, and J. R. Haak, *J. Chem. Phys.*, 1984, **81**, 3684–3690.

21. J. P. Ryckaert, G. Ciccotti, and H. J. C. Berendsen, *J. Comput. Phys.*, 1977, **23**, 327–341.

22. T. Darden, D. York, and L. Pedersen, *J. Chem. Phys.*, 1993, **98**, 10089–10092.

23. D. R. Roe and T. E. Cheatham III, *J. Chem. Theory. Comput.*, 2013, **9**, 3084–3095.

24. W. Humphrey, A. Dalke, and K. Schulten, *J. Mol. Graph.*, 1996, 14, 33–38.